ACS APPLIED MATERIALS & INTERFACES

Research Article

www.acsami.org

Preparation and Properties of Electrospun Soy Protein Isolate/Polyethylene Oxide Nanofiber Membranes

Xuezhu Xu,[†,‡] Long Jiang,*[,†] Zhengping Zhou,[†] Xiangfa Wu,[†] and Yechun Wang[†]

[†]Department of Mechanical Engineering and [‡]Program of Materials and Nanotechnology, North Dakota State University, PO Box 6050, Fargo, North Dakota 58108, United States

ABSTRACT: Soy protein isolate (SPI) and polyethylene oxide (PEO) were dissolved in 1,1,1,3,3,3-hexafluoro-2-propanol (HFIP) and nonwoven nanofiber membranes were prepared from the solution by electrospinning. PEO functioned as a cospinning polymer in the process to improve the spinnability of SPI. The ratio of SPI to PEO was varied and the rest spinning conditions remained unchanged. The morphology of the nanofiber membranes, SPI and PEO distribution and phase structure in the fiber, crystallization and interaction between SPI and PEO, thermal properties and wettability of the membranes were studied. The results showed that the diameter of most of the nanofibers was in the range of 200−300 nm. SPI and PEO showed high compatibility in the fiber and SPI was homogeneously dispersed at nanoscale. Crystallization of SPI and PEO in the fiber was significantly different from that of their pure forms. All the nanofiber membranes showed superhydrophilicity. These nanofiber membranes can find importance in filtration and biomedical applications.

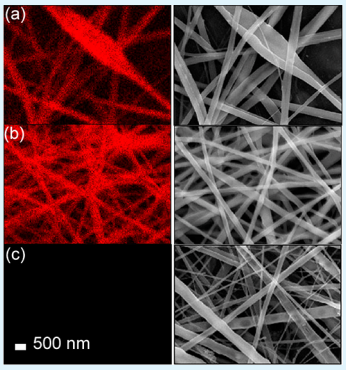

KEYWORDS: *Soy protein isolate, polyethylene oxide, electrospinning, nanofibers, wettability*

1. INTRODUCTION

Intensive research on electrospun nanofiber membranes has been conducted in recent years. These nanofiber membranes have shown great potentials in applications such as antimicrobial active packaging, tunable hydrophobicity and water adhesion, air filtration, tissue scaffolds for tissue engineering, drug delivery, biosensors, and enzyme immobilization, and so on.[1−6] Many review papers in this field provide in-depth information about the principles, processing and applications of electrospinning and electrospun fibers.[7−11] Electrospinning is a facile and increasingly cost-effective method to produce nanofibers. Fiber diameter and fiber mat architectures are tunable by varying the process and material parameters such as cospinning polymer, solution viscosity and conductivity, voltage, flow rate, nozzle-collector distance, and collection methods. Electrospun nanofibers offer many advantages over traditional fibers including high surface area to volume ratio, tunable porosity, and ease of manipulating fiber chemical compositions and structures for desired properties and functionalities. Many synthetic polymer materials such as nylon, polyethylene terephthalate (PET), polyethylene glycol (PEG), and polyacrylonitrile (PAN) have been electrospun into nanofibers with the diameter in the range of tens of nanometers to a few micrometers.[12−14] In recent years, electrospinning of naturally occurring biopolymers including mostly polysaccharides (cellulose, chitin, chitosan, alginate, dextran, etc.), proteins (collagen, gelatin, silk, casein, wheat protein, zein, egg albumen, human and bovine fibrinogen, wool, etc.), DNA, and their blends with other polymers have been intensively studied because of their biodegradability, biocompatibility and renewability. Comprehensive reviews about electrospun nanofibers of the naturally occurring biopolymers has been published by Schiffman and Schauer.[15,16] Readers are suggested to study these two reviews for more detailed information in this field.

Soy protein is a low cost plant protein in abundant supply. Soy protein has been shown to be suitable for biomedical applications.[17−21] Electrospinning of pure soy protein has been proven difficult. Soy protein does not dissolve in common organic solvents. Rather, it dissolves in aqueous media with a pH-value higher or lower than its isoelectric point (about 4−5). The ionic strength of the media varies its solubility.[22,23] NaOH aqueous solutions are the most commonly used solvent for soy protein electrospinning. A cospinning polymer, e.g., polyvinyl alcohol (PVA),[24] PEO,[25] PAN,[26] and zein,[27] had to be used to increase the spinnability of the soy protein solutions.

HFIP is an organic polar solvent which is capable of dissolving many polymers (e.g., polyamides, polyketones, etc.) that are not soluble in common organic solvents. HFIP can also dissolve biopolymers such as chitin and silk. It was used as the solvent in electrospinning of the two biopolymers.[28,29] Using HFIP as the solvent for soy protein electrospinning is relatively new. Very recently, Lin compared the effects of aqueous NaOH solution and HFIP on the properties of electrospun SPI/PEO nanofibers.[4] The author found that the nanofibers spun from HFIP solutions were tougher and resistant to aqueous mediums without cross-linking. Scaffolds made of these nanofibers have been tested for fiber diameter and surface quality, mechanical properties, biocompatibility, in vitro degradation and interactions with human dermal fibroblasts. Potential benefits of using the SPI/PEO scaffolds as wound healing materials were

Received: June 2, 2012
Accepted: July 27, 2012
Published: July 27, 2012

   dx.doi.org/10.1021/am300991e | ACS Appl. Mater. Interfaces 2012, 4, 4331−4337

discovered from the results. However, in-depth material characterizations on these nanofibers were not performed.

SPI has shown great potential as a raw material for electrospinning. SPI is renewable, economical, and biocompatible. SPI nanofiber membranes have potential applications ranging from filtration to biomedical products. However, studies on electrospinning of SPI are still scarce. Many properties of the SPI nanofiber membranes have not been explored. Electrospinning of soy protein remains difficult due to the polyelectrolytic nature of polypeptide molecules. In this study, soy protein nanofiber membranes were prepared using electrospinning. HFIP and PEO were used as the solvent and cospinning polymer, respectively. Properties of the nanofiber membranes including morphology, phase structure, thermal properties, crystallization, and wettability were studied. The results are expected to provide important knowledge of the electrospun SPI/PEO nanofibers and facilitate the development of novel SPI nanofiber-based products for broad applications.

2. MATERIALS AND METHODS

Materials. Soy protein isolate (PRO-FAM 974) was provided by Archer Daniels Midland Company. It mainly consists of protein (90%), fat (4%), ash (5%), and some carbohydrates (<1%). 1, 1, 1, 3, 3, 3 hexafluoro-2-propanol (HFIP) (Sigma-Aldrich) was used as the solvent for SPI. Polyethylene oxide from Sigma-Aldrich (M_v 200 000) was used as the cospinning polymer.

Procedures and Characterizations. 0.075 g PEO was added into 15 mL HFIP to obtain a 0.5% (w/v) solution. 1.2, 0.75, 0.45, and 0.15 g of SPI were added to the solution to obtain final SPI:PEO mass ratios of 16:1, 10:1, 6:1, and 2:1, respectively. All the solutions were stirred using a magnetic hot plate stirrer (VWR) (40 °C, 400 rpm) for 8 days to achieve complete dissolution.

SPI/PEO nanofibers were prepared using single-needle based electrospinning. Eight ml of each solution was loaded into a syringe equipped with a 22-gauge blunt-tipped needle. An aluminum foil positioned 25 cm apart from the needle was used as the fiber collector. A DC voltage of 25 kV was applied between the needle and the collector. A flow rate of 1.5 mL/min was maintained using a digital syringe pump. For comparison, pure PEO nanofibers were also prepared using the same spinning conditions.

A JEOL 7600F field-emission scanning electron microscopy (FESEM) operating at 2.00 kV was used to study membrane morphology. A small piece of electrospun nanofibe membrane was cut and attached to an aluminum mount using silver paint. The sample was then coated with a thin layer carbon using a Cressington 208C carbon coater. For each sample, 10 images were taken from randomly selected areas. At least 100 individual fibers were chosen from each image to measure their diameters using ImageJ image processing and analysis software. The obtained values were analyzed for diameter distribution of the fibers. The energy-dispersive X-ray spectrometer (EDS) mounted on the FESEM was used to obtain elemental mapping for the electrospun nanofibers. The magnification of 16 000 and accelerating voltage of 8.0 kV were used for the mapping process. Three different regions of each membrane were analyzed by the EDS and elemental contents of these regions were calculated.

A Thermo Fisher Scientific Fourier Transform Infrared Spectrometer (FT-IR) (Model: 4700/5700/6700/8700) was used to obtain molecular bonding information of the samples. The samples were dried in an oven, ground with KBr and pressed into discs for the tests. The spectra were recorded from 400 to 4000 cm^{-1} at 1.928 cm^{-1} resolution. A total of 32 repetitive scans were performed for each sample.

Wide angle X-ray diffraction patterns were obtained using an X-ray powder diffractometer (Philips X'Pert MPD) equipped with a vertically mounted goniometer and a Cu Kα X-ray source. The diffractometer operated at 45 kV and 40 mA. The scan started from 2.5° at a rate of 0.05°/s. Nanofiber membranes were directly mounted on the sample stage without being ground into powder.

A Q1000 differential scanning calorimeter (DSC) from TA Instruments was used to examine thermal properties of pure PEO, raw SPI, and SPI/PEO nanofibers. The samples were sealed in aluminum pans and scanned from −30 to 300 at 10 °C/min heating rate. Nitrogen flow was supplied at 50 mL/min during the scan.

Thermal stability of the fibers was evaluated using a TA Q500 thermo gravimetric analyzer (TGA). The samples were put in a platinum holder and scanned from 20 to 700 at 20 °C/min heating rate. Nitrogen flow was supplied at 60 mL/min during the test.

Wettability of the nanofiber membranes was evaluated using a contact angle and surface tension instrument (FTA1000 B Class by First Ten Angstroms, Inc.). A droplet of ethanol with controlled volume was deposited on the membrane surface. Shape evolution of the droplet was monitored using a high speed camera operating at 250 frames per second. Analyses of the drop shape and contact angle measurements were performed using the accompanying software of the instrument.

3. RESULTS AND DISCUSSION

3.1. Morphology. The micrographs of SPI/PEO nanofibers with four different SPI:PEO ratios (i.e., 16:1, 10:1, 6:1 and 2:1) are shown in Figure 1. When the SPI concentration was high

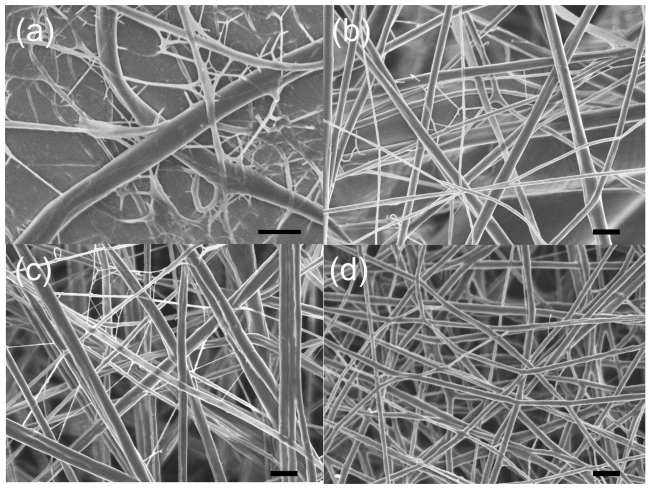

Figure 1. FESEM images of SPI/PEO nanofiber membranes (a) 16:1; (b) 10:1; (c) 6:1; (d) 2:1. Scale bar in each image is 1 μm.

(16:1), the fibers demonstrated large diameter, wide diameter distribution, and irregular structures. Branching of the fibers was significant (Figure 1a). In-flight splitting/splaying/branching of polymer jets during spinning have been observed on many polymer solutions, especially at high polymer concentrations.[30−32] The branching is attributed to uneven distribution of the charge carried by the jets, which is caused by jet elongation/bending and solvent evaporation. The jets can reduce their local surface charge density by ejecting smaller jets from the surface of the primary jets or by splitting into multiple smaller jets. SPI exhibits net charge in its solvents due to the different strength of basicity and acidity of the $-NH_2$ and −COOH groups in SPI molecules. Higher SPI concentration could potentially lead to more uneven jet surface charge distribution, which consequently resulted in higher probability of jet branching. At the lower SPI concentrations (i.e., 10:1, 6:1, and 2:1), the fibers were more uniform, continuous and smooth due to improved charge distribution and solution homogeneity (Figure 1b−d).

One hundred fibers were randomly selected from 16:1, 10:1, 6:1, and 2:1 nanofibers to calculate their average diameter and diameter distribution (Figure 2). It is evident from the figure

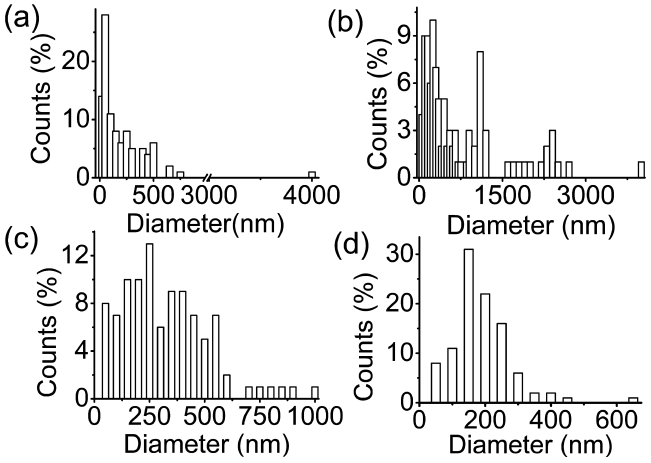

Figure 2. Histograms of SPI/PEO nanofiber diameter (a) 16:1; (b)10:1; (c) 6:1; (d) 2:1.

that the first three fibers showed bimodal diameter distribution and the distribution transitioned to unimodal distribution with decreasing SPI concentration. For SPI/PEO 16:1, the primary fibers were the small branches from the big fibers (Figure 2a), which exhibited a mean diameter of 195 ± 166 nm and accounted for 97% of the total fiber population. The big fibers showed a mean diameter of 2740 ± 2040 nm and they only accounted for 3% of the total population (though their volume ratio was far larger than that of the small branches). For SPI/PEO 10:1, the mean diameters for the primary (74% population) and secondary (26% population) fibers were 352 ± 218 and 1782 ± 763 nm, respectively. For SPI/PEO 6:1, the fibers exhibited more uniform diameter distribution: 353 ± 199 nm for the primary fibers (15%) and 1033 ± 110 nm for the secondary fibers (1%). Finally, for SPI/PEO 2:1, the fibers virtually exhibited a unimodal distribution with a mean diameter of 214 ± 89 nm, which was the lowest fiber diameter and the narrowest diameter distribution among all the fibers. The trend showed that PEO as the cospinning polymer indeed improved the spinnability of SPI and the quality of the obtained fibers.

The smooth fiber surfaces shown in Figures 1b, c and d imply that no obvious phase separation between SPI and PEO occurred during the electrospinning process. Good compatibility seemed to exist between the two phases. To confirm this, we used EDS to perform elemental analysis and elemental mapping on the fibers. Nitrogen atoms were unique to soy protein molecules in the fiber and were used to determine the distribution of SPI. The nanofibers with SPI/PEO ratios of 10:1 and 2:1were tested for SPI distribution and their nitrogen elemental mapping graphs are shown in Figure 3. Nitrogen was represented with red color in the graph. The 10:1 nanofibers demonstrate homogeneous dispersion of SPI (Figure 3a).

3.2. Crystalline Structure. Figure 4 shows the X-ray diffraction patterns of the nanofibers and their raw materials. Pure PEO powder exhibits two diffraction peaks at 19.2 and 23.3°, representing (120) and (112) planes, respectively.[33] However, PEO nanofibers only showed the diffraction peak at 19.2°, indicating that the spinning process affected the growth of PEO crystals. The new crystalline structure was presumably

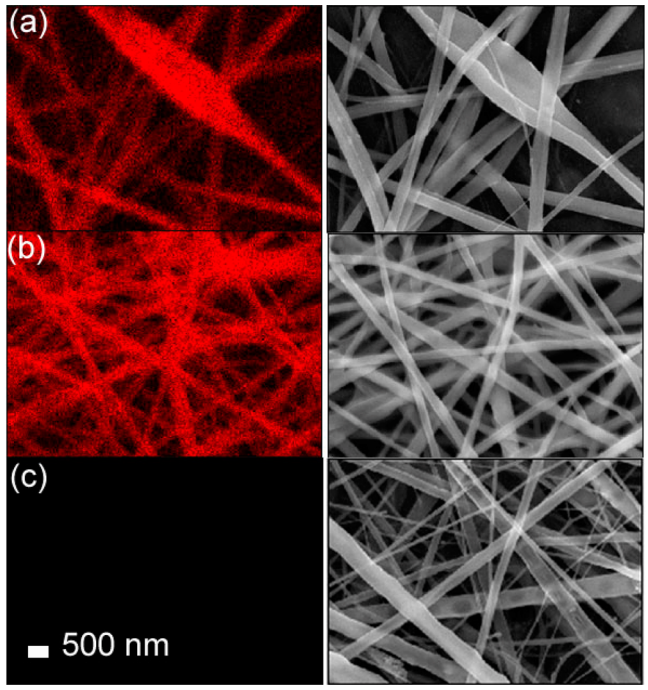

Figure 3. Elemental mapping of nitrogen by EDS. (a) SPI/PEO 10:1; (b) SPI/PEO 2:1;(c) neat PEO nanofibers.

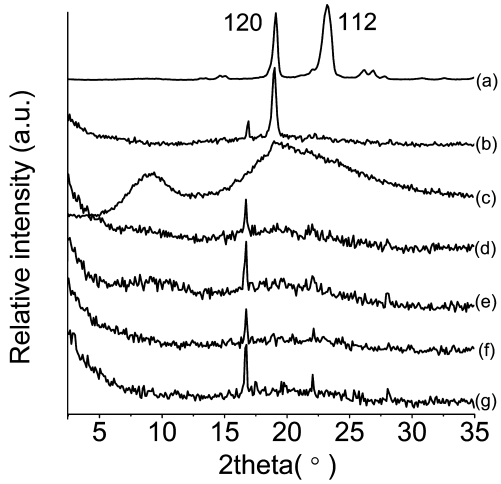

Figure 4. XRD diffraction patterns of (a) pure PEO powder, (b) pure PEO nanofiber membrane, (c) raw SPI powder, SPI/PEO nanofiber membranes with SPI: PEO ratios of (d) 10:1, (e) 6:1, and (f) 2:1. (g) Diffraction pattern of the aluminum foil used for nanofiber collection. It shows that the peak at ca. 17° of curves b, d, e, and f was from the aluminum foil substrate.

associated with small diameter of the nanofibers. PEO powder has a monoclinic crystalline structure with its (120) planes parallel to the PEO chain direction and (112) planes intersecting the chain direction. The small diameter of the nanofibers limited the size of (112) planes and therefore reduced or even eliminated their diffractions. Deitzel et al. also reported reduced (112) diffraction of electrospun PEO nanofibers. Strong diffraction of SPI powder occurred at 9.2 and 19.3°, which were in agreement with other reports.[34,35] Crystallization of PEO and SPI in SPI/PEO nanofibers was different from that in their pure forms. The diffraction peaks of SPI at both 9.2 and 19.3° were greatly depressed in the SPI/

PEO nanofibers, implying that the original protein microstructures were largely destructed by the solvent and these structures were not recovered in the nanofibers. Neither of the PEO diffraction peaks appeared in the diffraction patterns of the nanofibers, indicating that the PEO in the nanofibers was dominantly amorphous. The depression or complete disappearance of the diffraction peaks in composites was also reported by other researchers. Wang et al. reported a gradually disappearing peak associated with alginate in alginate/soy protein composites.[34] Su et al. discovered that the intensity of the diffraction peaks of PVA and SPI decreased significantly at 20 wt % PVA contents in PVA/SPI blends.[35] The depression of material crystallization in a composite is commonly explained by the interference from other components of the composite. The regular folding of polymer chains during crystallization can be interrupted by another species of polymer chains when the two types of chains are miscible and interact closely. Quick solvent evaporation in electrospinning was another reason contributing to the amorphous structure of the nanofibers. SPI and PEO were unable to fully crystallize before the nanofibers solidified.

3.3. Thermal Properties. DSC and TGA tests were performed to study the crystallization and thermal properties of the nanofibers. DSC thermograms of pure PEO powder, PEO nanofibers, SPI powder, and 10:1 and 6:1 SPI/PEO nanofibers are shown in Figure 5. Pure PEO powder exhibited a sharp

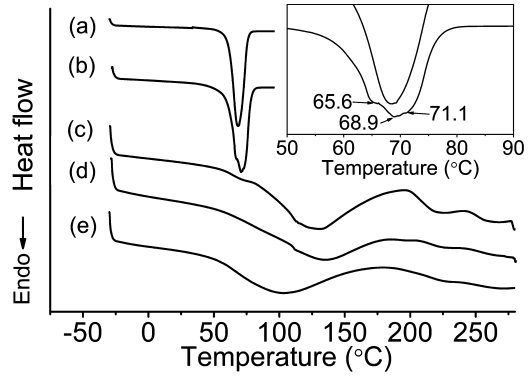

Figure 5. DSC thermograms of (a) pure PEO powder, (b) PEO nanofiber membrane, (c) raw SPI powder, (d) SPI/PEO 10:1, and (e) SPI/PEO 6:1 nanofiber membranes. The inset compares the melting peaks of the PEO powder and the PEO nanofiber membrane.

melting peak at 68.4 °C with an enthalpy of 192.9 J/g. By contrast, the melting curve of PEO nanofibers includes a peak and two shoulders on each side (inset in Figure 5), indicating multiple populations of crystalline fractions. The melting peak of the nanofibers was at the same temperature as that of the powder. Both peaks were attributed to the melting of unoriented spherulites consisting of folded chain lamellae. The low-temperature shoulder was due to the melting of defect-ridden spherulites. These spherulites occurred in the nanofibers because of fast evaporation of the solvent. The high-temperature shoulder was presumed to be attributed to the melting of oriented crystals. The extensional flow during electrospinning aligned polymer chains in the fiber direction. These extended chains formed crystals that showed higher melting point than ordinary spherulites.[36] The enthalpy of fusion of the nanofibers (172.3 J/g) was lower than that of the powder, indicating lower crystallinity of the nanofibers due to quick evaporation of the solvent.

Below 200 °C raw SPI powder showed a weak (68.3 °C) and a strong (127.2 °C) endothermic transition. Scilingo et al. also reported two endothermic transitions (76.0 and 91.5 °C) for SPI and attributed them to denaturation of 7S (conglycinin) and 11S (glycinin) fractions of soy protein, respectively.[37] SPI contains a range of protein fractions (e.g., 2S, 7S, 11S, and 15S) with molecular weight ranging from 8 to 600 kDa. 7S and 11S are the two major components.[38] We postulate that the endothermic transitions occurring at 68.3 and 127.2 °C in this study were caused by the denaturation of 7S and 11S proteins, respectively. The different denaturation temperatures observed in this study were due to different DSC test methods. In Scilingo's study SPI suspension in water was tested whereas SPI dry powder was tested in this work. Water as a hydrophilic solvent interacts with the proteins and facilitates their denaturation (i.e., decreases their denaturation temperatures).[39] The weak transition of 7S observed in this study could imply that the denaturation of 7S was insignificant when the moisture level of the protein was low. It was also possible that the content of 7S was low in the SPI sample because of the way it was produced.[40] At present we are not clear about the exact origins of the thermal transitions at higher temperatures (about 220 and 260 °C). They may be attributed to the denaturation of higher molecular weight soy proteins, or more likely to the thermal decomposition of some fractions of the proteins as will be demonstrated in TGA curves.

No PEO melting can be observed from the DSC curves of the SPI/PEO nanofiber membrane (Figures 5). In a polymer blend system, this often means that the components of the blend are miscible with each other. The good miscibility between SPI and PEO was also demonstrated by the SEM/EDS and XRD results discussed earlier. The presence of PEO in the nanofibers also caused other effects on the thermal behavior of SPI. The most obvious one was that the denaturation of 11S was shifted to a lower temperature for the 6:1 nanofibers (Figure 5). When the temperature was above its melting point, PEO could act as a polymeric solvent in the nanofibers and facilitated the denaturation of 11S, in a similar way as water did. For the weak transitions of the SPI powder (e.g., 7S and the ones at 220 and 260 °C), the presence of PEO in the nanofibers alleviated the intensities of these transitions, possibly due to a dilution effect.

TGA curves and their first derivatives (DTG) for pure PEO, SPI powder and SPI/PEO nanofiber membranes are shown in Figures 6 and 7, respectively. The pure PEO was stable below 200 °C, followed by a two-stage decomposition which was evident in Figure 7. It decomposed completely at 412 °C. The

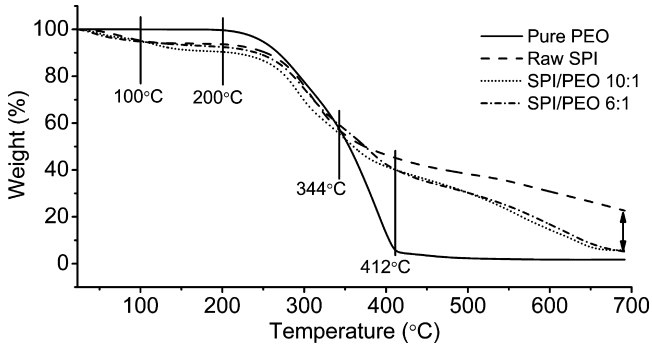

Figure 6. TGA curves of pure PEO powder, raw SPI powder, SPI/PEO 10:1, and SPI/PEO 6:1 nanofiber membranes.

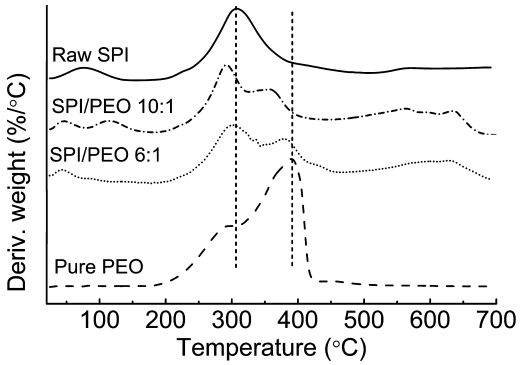

Figure 7. DTG curves of pure PEO powder, raw SPI powder, SPI/PEO 10:1, and SPI/PEO 6:1 nanofiber membranes.

SPI powder lost approximate 6% weight at 100 °C mainly due to moisture evaporation. It was relatively stable between 100 and 200 °C and exhibited a maximum decomposition rate at 305 °C. Its weight continued to drop until the temperature reached the maximum temperature (700 °C). According to a prior research,[41] the decomposition occurring blew ~400 °C was mainly attributed to the breakage of the peptide bonds. S−S, O−N, and O−O linkages started to sever at higher temperatures and the decomposition continued until only ashes were left. For the SPI/PEO nanofibers, low temperature weight loss (<100 °C) was due to moisture and residual solvent evaporation. The samples showed two peaks between 200 and 420 °C in DTG, a combined result from the decomposition of SPI and PEO (Figure 7). However, the two peaks were not a direct superposition of the peaks of the pure SPI and PEO. For instance, the decomposition temperature of SPI seemed to be decreased in the nanofibers, an indication of the influences from the PEO phase.

The decomposition rate of the SPI/PEO nanofibers was also higher than that of the SPI powder after 344 °C (Figure 6). The reason could be 2-fold. First the SPI in the nanofibers had lost most of its folded structure as revealed by XRD. This loss made SPI more vulnerable to thermal decomposition. Second the degradation of PEO opened pores in the nanofibers. The porous structure facilitated heat and mass transfer and therefore accelerated SPI decomposition.

3.4. FT-IR. FT-IR spectra were obtained to determine the potential interactions between SPI and PEO (Figure 8). PEO powder showed a characteristic triplet (1148, 1110, and 1062 cm^{-1}) with a maximum at 1110 cm^{-1}, which was associated with C−O−C vibration.[42] This triplet depends strongly on the crystallinity of PEO and the intermolecular interactions (e.g., hydrogen bonding) between C−O−C and other groups in a PEO containing blend. C−O−C is a proton acceptor and may form hydrogen bonding with proton donors such as OH, NH and NH_2 groups in soy protein molecules.[43] It was evident that on the spectra of 10:1 and 6:1 SPI/PEO nanofibers the triplet completely disappeared. The disappearance could be attributed to the lack of PEO crystalline structures in the nanofibers (which had been confirmed by the results from the XRD and DSC tests) due to the strong interactions between SPI and PEO and the enhanced miscibility between the two phases.[44] SPI powder showed absorptions at 1590 cm^{-1} (C═O stretching, amide I), 1450 cm^{-1} (N−H bending, amide II), and 1160 cm^{-1} (combination of N−H bending and C−N stretching, amide III). Amide II absorption was shifted to a higher wavenumber in the SPI/PEO nanofibers and amide III

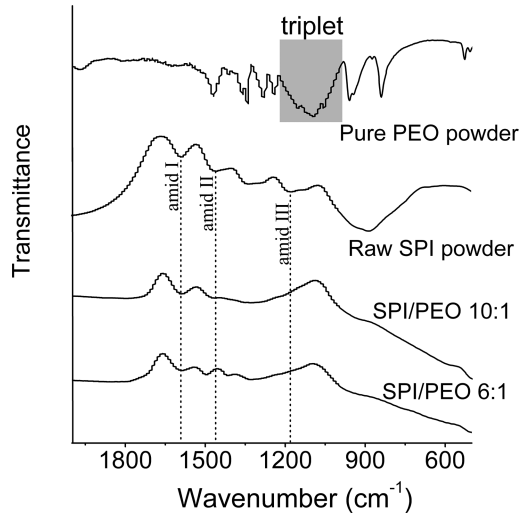

Figure 8. FT-IR spectra of the pure PEO powder, raw SPI powder, and nanofiber membranes with 10:1 and 6:1 SPI/PEO ratios.

absorption disappeared from the spectra, both of which could be attributed to the hydrogen bonding between N−H and C−O−C.

3.5. Wettability. Wettability of a solid material is mainly determined by its surface chemical composition and surface topography. Conventionally, the degree of wettability is classified into several levels by using the contact angle θ of the material surface. For a surface with 25° < θ < 90°, the material is considered to exhibit high wettability. For 90° < θ < 150°, the material possesses low wettability. The material is considered superhydrophilic if its contact angle is lower than 25°, whereas the material is superhydrophobic if the angle is larger than 150°.[45] The wettability of the SPI/PEO nanofiber membranes were tested by depositing an ethanol droplet on the membrane surfaces and following its edge profile. It should be emphasized that the method of analyzing the shape of a test droplet placed on a surface is best suited for the measurement of the contact angles of solid nonabsorptive surfaces. Although the nanofiber membranes were absorptive materials, this method was still used in this study to demonstrate the rate of spreading and absorption of the droplet on the nanofiber membranes. The values of "contact angle" measured below indicated the degree of liquid spreading and absorption on the membrane surfaces.

The evolution of the edge profiles on three different nanofiber membrane surfaces is given in Figure 9. It was evident that the ethanol droplets spread and got absorbed by the nanofiber membranes at different rates. The 10:1 nanofiber membrane showed the shortest spreading time before the droplet became completely flat.

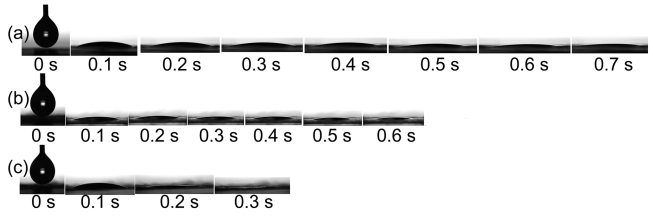

Figure 9. Images of an ethanol droplet on (a) SPI/PEO 2:1, (b) SPI/PEO 6:1, (c) SPI/PEO 10:1.

The "contact angles" for different nanofiber membranes were measured from the images of the ethanol droplets. The angles were plotted as a function of time in Figure 10. The initial

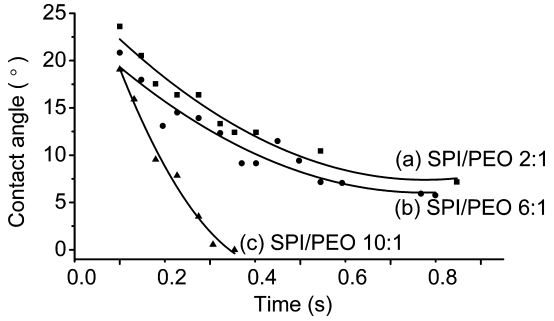

Figure 10. Evolution of the "contact angle" of ethanol droplets on (a) SPI/PEO 2:1; (b) SPI/PEO 6:1; and (c) SPI/PEO 10:1 nanofiber membranes.

"contact angles" for SPI/PEO 2:1, 6:1, and 10:1 was 38.29, 30.29, and 33.55°, respectively. The initial angles were similar to each other despite the different chemical compositions and morphologies among the membranes. The measurable ultimate "contact angles" for all the membranes were lower than 10°, an indication of superhydrophilic property by the conventional definition. The time periods required to achieve the ultimate angle were shorter than one second, indicating fast ethanol spreading and absorption.

Developed to calculate the contact angle of a rough surface (i.e., apparent contact angle), the Wenzel's model can be used to understand the high spreading and absorption rate of the nanofiber membranes. The contact angle of a rough surface is defined by the following equation:[46]

$$\cos \theta* = r\cos \theta$$

where θ* is the apparent contact angle at equilibrium state; r is the roughness ratio, which is the ratio of the true area to the apparent area of the surface (always larger than 1 for a rough surface); θ is the Young's contact angle for the ideal surface of the same material. According to this equation, surface roughness plays an important role in wettability. For a hydrophilic material with a contact angel in the range of $0° < \theta < 90°$, because r is larger than 1, cos θ* is then larger than cos θ, and thus θ* is smaller than θ. As a result, the surface becomes more hydrophilic when its roughness increases. However, for a hydrophobic material with a contact angel in the range of $90° < \theta < 180°$, cos θ* is smaller than cos θ, and so θ* is larger than θ. This results in more hydrophobic surface. These two opposite effects of roughness on surface wettability have been demonstrated on electrospun nanofiber membranes by Yang et al.[47] Besides surface roughness, surface chemical composition is another important factor. Polar groups on the surface increase the interactions between the surface and polar liquids and thus increase surface wettability. Therefore, both surface roughness and chemical composition can be used to control surface wettability of a material. In the case of the SPI/PEO membranes, SPI contained numerous polar groups from various amino acids, which made it inherently hydrophilic. The nanoporous structure of the membranes caused a very large roughness ratio. These two reasons jointly led to the high wettability of the nanofiber membranes under consideration. The superhydrophilicity of the membranes can be very useful for biomedical applications such as wound dressing. Wound exudates can be absorbed efficiently and the wound healing process can be accelerated when such nanofiber membranes are used. If necessary, water resistance of these membranes can be improved by applying cross-linking agents (e.g., glutaraldehyde, citric acid, etc.) through sample immersion or vapor treatments.

4. CONCLUSIONS

In this research, nanofiber membranes with soy protein as the major ingredient were produced using electrospinning. PEO was used as a cospinning polymer to improve the spinning stability and fiber quality. SPI:PEO ratio was varied and its effects on fiber quality, crystallization, thermal property, and wettability of the membranes were investigated. Quality nanofibers with a SPI:PEO ratio up to 10 could be achieved. SPI and PEO were found to be miscible with each other in the nanofibers based on the results of phase structure, crystallization, chemical group interactions, and thermal properties of the fibers. All the SPI/PEO nanofiber membranes showed superhydrophilicity, a desirable property for many applications.

AUTHOR INFORMATION

Corresponding Author

*E-mail: long.jiang@ndsu.edu. Tel: 1 701 231 9512.

Notes

The authors declare no competing financial interest.

ACKNOWLEDGMENTS

North Dakota Experimental Program to Stimulate Competitive Research (ND EPSCoR) is greatly appreciated for funding this research. The authors thank Archer Daniels Midland Company for providing soy protein isolate.

REFERENCES

(1) Vega-Lugo, A. C.; Lim, L. T. *Food Res. Int.* **2009**, *42*, 933−940.
(2) Pisuchpen, T.; Chaim-ngoen, N.; Intasanta, N.; Supaphol, P.; Voravee, P.; Hoven, V. P. *Langmuir* **2011**, *27*, 3654−3661.
(3) Heikkilä P. Nanostructured Fibre Composites, and Materials for Air Filtration. *Ph.D. thesis*, Tempere University of Technology, Tampere, Finland, 2008.
(4) Lin, L. Electrospun Soy Protein-based Scaffolds for Skin Tissue Engineering and Wound Healing. *Ph.D. thesis*, Drexel University, Philadelphia, PA, 2011.
(5) Qi, H.; Hu, P.; Xu, J.; Wang, A. *Biomacromolecules* **2006**, *7*, 2327−2330.
(6) Patel, A. C.; Li, S.; Yuan, J. M.; Wei, Y. *Nano Lett.* **2006**, *6* (5), 1042−1046.
(7) Dzenis, Y. A. *Science* **2004**, *304*, 1917−1919.
(8) Huang, Z. M.; Zhang, Y. Z.; Kotaki, M.; Ramakrishna, S. *Compos. Sci. Technol.* **2003**, *63*, 2223−2253.
(9) Li, D.; Xia, Y. *Adv. Mater.* **2004**, *16* (14), 1151−1170.
(10) Greiner, A.; Wendorff, J. H. *Angew. Chem.* **2007**, *46*, 5670−5703.
(11) Reneker, D. H.; Yarin, A. L.; Zussman, E.; Xu, H. *Adv. Appl. Mech.* **2007**, *41*, 43−195.
(12) Ma, Z.; Kotaki, M.; Yong, T.; He, W.; Ramakrishna, S. *Biomaterials* **2005**, *26*, 2527−2536.
(13) Bhattarai, S. R.; Bhattarai, N.; Yi, H. K.; Hwang, P. H. *Biomaterials* **2004**, *25*, 2595−2602.
(14) Yoon, H.; Kim, K.; Wang, X.; Fang, D.; Hsiao, B. S.; Chu, B. *Polymer* **2006**, *47*, 2434−2441.
(15) Schiffman, J. D.; Schauer, C. L. *Polymer Rev.* **2008**, *48*, 317−352.
(16) Kriegel, C.; Arrechi, A.; Kit, K.; McClements, D. J.; Weiss, J. *Crit. Rev. Food Sci. Nutr.* **2008**, *48* (8), 775−797.
(17) Silva, G. A.; Vaz, C. M.; Coutinho, O. P.; Cunha, A. M.; Reis, R. L. *J. Mater. Sci. Mater Med.* **2003**, *14* (12), 1055−66.

(18) Silva, S. S.; Santos, M. L.; Continho, O. P.; Mano, J. F.; Reis, R. L. *J. Mater. Sci. Mater. Med.* **2005**, *16* (6), 575−579.
(19) Vaz, C. M.; De Graaf, L. A.; Reis, R. L.; Cunha, A. M. *Int. J. Pharm.* **2008**, *355* (1−2), 1−18.
(20) Vaz, C. M.; De Graaf, L. A.; Reis, R. L.; Cunha, A. M. *Polym. Degrad. Stabil.* **2003**, *81*, 65−74.
(21) Vaz, C. M.; van Doeveren, P. F.; Reis, R. L.; Cunha, A. M. *Biomacromolecules* **2003**, *4* (6), 1520−1529.
(22) Rhim, J. W.; Gennadios, A.; Handa, A.; Weller, C. L.; Hanna, M. A. *J. Agric. Food Chem.* **2000**, *48*, 4937−4941.
(23) Renkema, J. M. S.; Gruppen, H.; Vliet., T. V. *J. Agric. Food Chem.* **2002**, *50*, 6064−6071.
(24) Cho, D.; Nnadi, O.; Netravali, A.; Joo, Y. L. *Macromol. Mater. Eng.* **2010**, *295*, 763−773.
(25) Vega-Lugo, A. C.; Lim, L. T. *J. Biobased Mater. Bio.* **2008**, *2*, 223−230.
(26) Yu, L.; Yan, D.; Sun, G.; Gu, L. *J. Appl. Polym. Sci.* **2008**, *108*, 1100−1108.
(27) Phiriyawirut, M.; Rodchanacheewa, N.; Nensiri, N.; Supaphol, P. *Adv. Mater. Res.* **2008**, *55*−*57*, 733−736.
(28) Park, K. E.; Kang, H. K.; Lee, S. J.; Min, B. M.; Park, W. H. *Biomacromolecules* **2006**, *7*, 635−643.
(29) Min, B. M.; Jeong, L.; Lee, K. Y.; Park, W. H. *Macromol. Biosci.* **2006**, *6*, 285−292.
(30) Koombhongse, S.; Liu, W. X.; Reneker, D. H. *J. Polym. Sci., Part B: Polym. Phys.* **2001**, *39*, 2598−606.
(31) Deitzel, J. M.; Kleinmeyer, J.; Harris, D.; Tan, N. C. B. *Polymer* **2001**, *42*, 261−72.
(32) Bergshoef, M, M; Vancso, G. *J. Adv Mater.* **1999**, *11* (16), 1362−5. Koombhongse, S.; Liu, W. X.; Reneker, D. H. *J. Polym. Sci., Part B: Polym. Phys.* **2001**, *39*, 2598−2606.
(33) Deitzel, J. M.; Kleinmeyer, J. D.; Kirvonen, J. K.; Tan, N. C. B. *Polymer* **2001**, *42*, 8163−8170.
(34) Wang, Q.; Du, Y.; Hu, X.; Yang, J.; Fan, L.; Feng, T. *J. Appl. Polym. Sci.* **2006**, *101*, 425−431.
(35) Su, J. F.; Huang, Z.; Yang, C. M.; Yuan, X. Y. *J. Appl. Polym. Sci.* **2008**, *110*, 3706−3716.
(36) Somani, R. H.; Yang, L.; Sics., I.; Hsiao, B. S.; Pogodina, N.; Winter, H. H.; Agarwal, P.; Fruitwala, H.; Tsou, A. *Macromol. Symp.* **2002**, *185*, 105−117.
(37) Scilingo, A. A.; Añón, M. C. *J. Agric. Food Chem.* **1996**, *44*, 3751−3756.
(38) Hermansson, A. M. *J. Texture Stud.* **1979**, *9*, 33−58.
(39) Zhong, Z. K.; Sun, X. S. *Cereal Chem.* **2000**, *77*, 495−500.
(40) Kilara, A.; Sharkasi, T. Y.; Morr, C. V. *Crit. Rev. Food Sci.* **1986**, *24* (4), 323−395.
(41) Swain, S. N.; Rao, K. K.; Nayak, P. L. *Polym. Int.* **2005**, *54*, 739−743.
(42) Pereira, R. P.; Rocco, A. M.; Bielschowsky, C. E. *J. Phys. Chem. B* **2004**, *108* (34), 12677−84.
(43) Rocco, A. M.; Moreira, D. P.; Pereira, R. P. *Eur. Polym. J.* **2003**, *39*, 1925−1934.
(44) Silva, E. F.; Pereira, R. P.; Rocco, A. M. *Eur. Polym. J.* **2009**, *45*, 3127−3137.
(45) Donaldson, E. C. In *Technology & Engineering*, 1st ed.; Donaldson, E. C., Alam, W., Eds.; Gulf Publication Company: Houston, TX, 2008; p 1−50.
(46) Wenzel, R. N. *Ind. Eng. Chem.* **1936**, *28* (8), 988−994.
(47) Yang, F.; Wolke, J. G. C.; Jansen, J. A. *Chem. Eng. J.* **2008**, *137* (1), 154−161.